CHAPTER 4

RESULTS AND DISCUSSION

4.1 Screening of enzymes

In this study, four types of thin films (Native-CRL, CMC-CRL, PVA-CRL and PVA:CMC-CRL) were screened to determine their catalytic efficiencies in the esterification between oleic acid and butanol. The amount of immobilized CRL used was made equivalent to the amount of protein in 50.0 mg of native CRL which was 1.08 mg protein. In general, the percentage of conversion was significantly different between native and immobilized CRL.

As shown in Figure 4.1, immobilized CRL showed percentage conversion of about 1.5 (PVA-CRL) – 3 (CMC-CRL) times higher than Native–CRL (8.9%). A similar finding was reported by Dalla-Vechia et al (2005). In their study, higher yields in n-pentyl laurate were obtained when lipases from *Mucor javanicus* (MJL) or *Rhyzopus oryzae* (ROL) were immobilized in CMC, PVA and a blend of CMC:PVA (70–99%), whereby lower yields were obtained using enzyme in a free form (6–33%). CRL immobilized onto CMC also showed a higher percentage conversion of ester which is 28.3% as compared to the other supports and native CRL. This is due to the dependence on a carbon number of the alkyl chain was observed. Higher yields (>10%) were observed for fatty acids with more than 10 carbon atoms.

These results showed that polymers such as PVA, CMC and CMC:PVA blends can be used successfully as alternative materials for lipase immobilization.

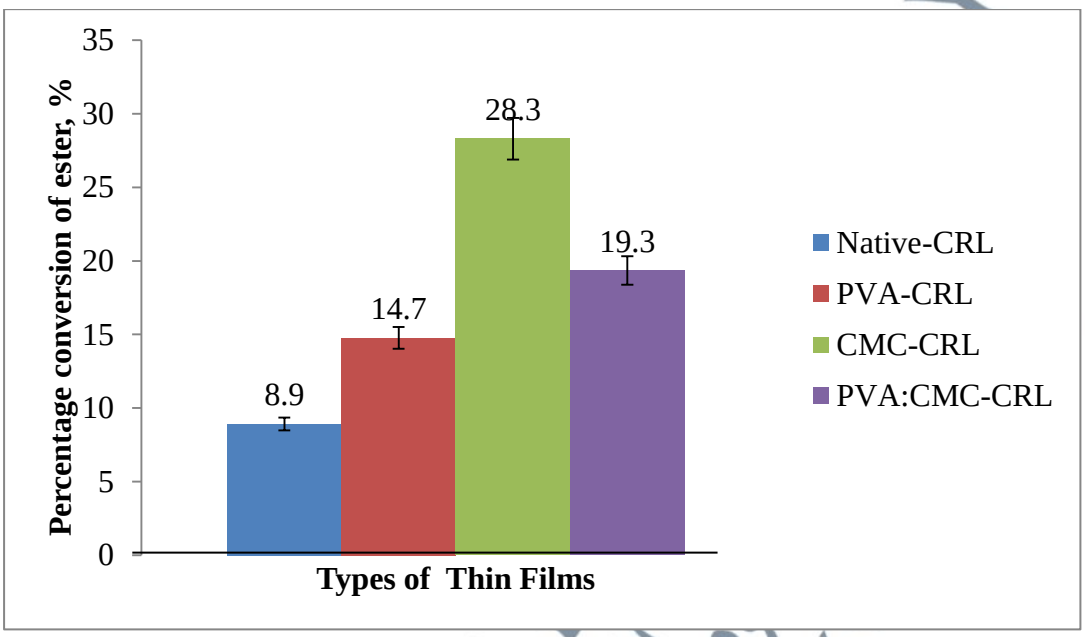

Figure 4.1: Graph of Percentage conversion of ester over the types of polymers

4.2 Characterization Using Scanning Electron Microscope (SEM)

Characterization using SEM on thin films with and without CRL was carried out to observe the surface morphologies of the support before and after immobilization. Figures 4.2-4.4 shows the SEM images between 1.00 kX magnifications.

As shown in Figure 4.2, the CMC thin film showed a clear plane surface, while the thin film containing CRL showed a mass of globular patterns on its surface, indicating the reposition of CRL on the support. Similarly, PVA also showed a clear plane surface when no CRL was entrapped into it [Figure 4.3(a)]. PVA containing CRL however showed an agglomeration on its surface [Figure 4.3(b)] as evidence of CRL entrapment within the thin film. A similar pattern was also observed for PVA:CMC

thin film without CRL [Figure 4.4(a)], where it showed a uniform layer, while the thin film with CRL immobilized onto it [Figure 4.4(b)] showed the globular structure of enzymes scattered on the surface of the thin film. All of these observations can be used as confirmation that immobilization of CRL had successfully taken place. Similar result was repeated by Hassan et al. (2015). In his study, the FESEM image with a magnification of 2.50 kX was captured after disserting the beads with surgical blade thereby revealing the native CRL globular shape.

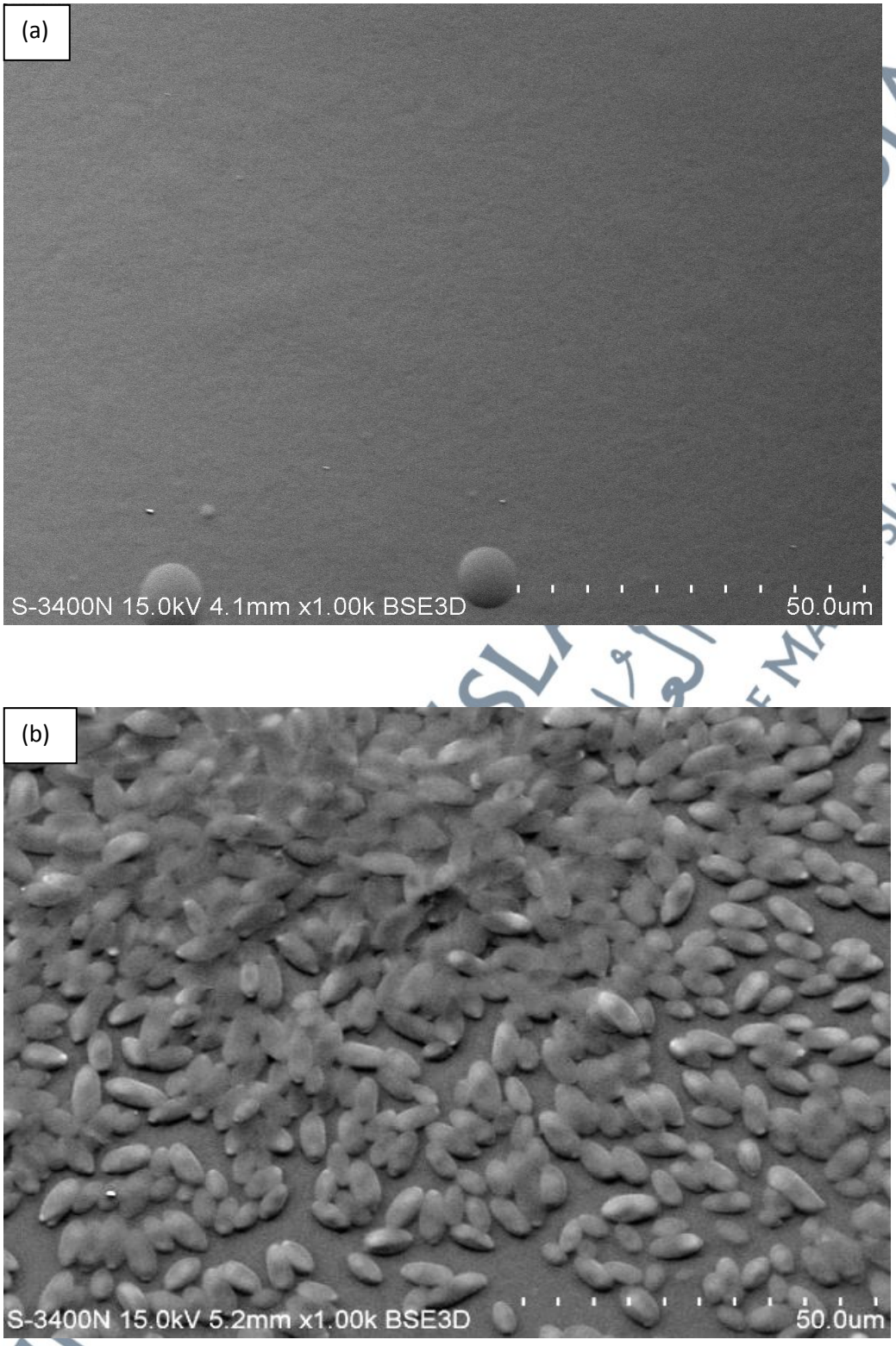

Figure 4.2: SEM images of (a) CMC thin film and (b) CMC-CRL

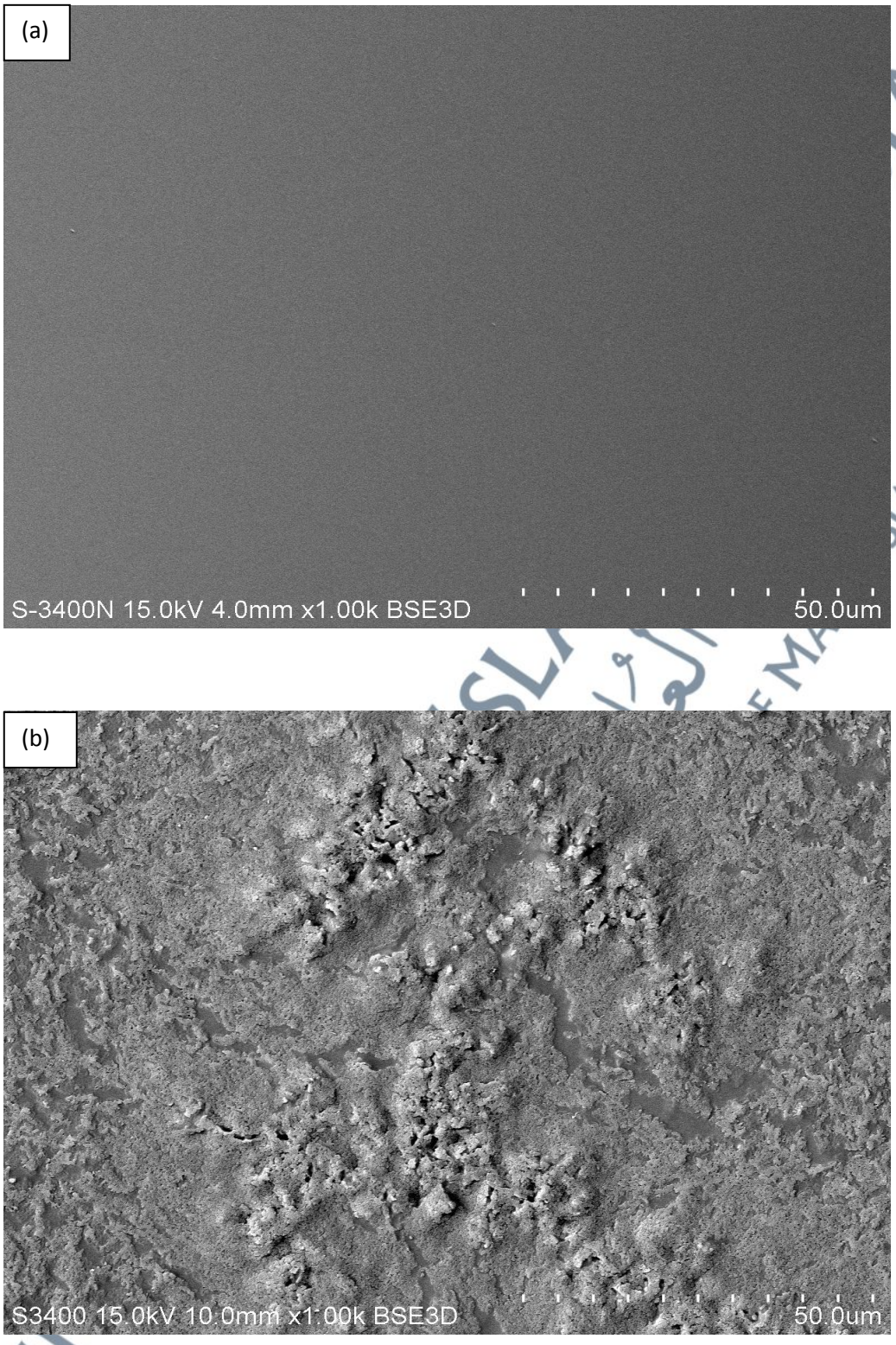

Figure 4.3: SEM images of: a) PVA thin film, and

b) PVA-CRL.

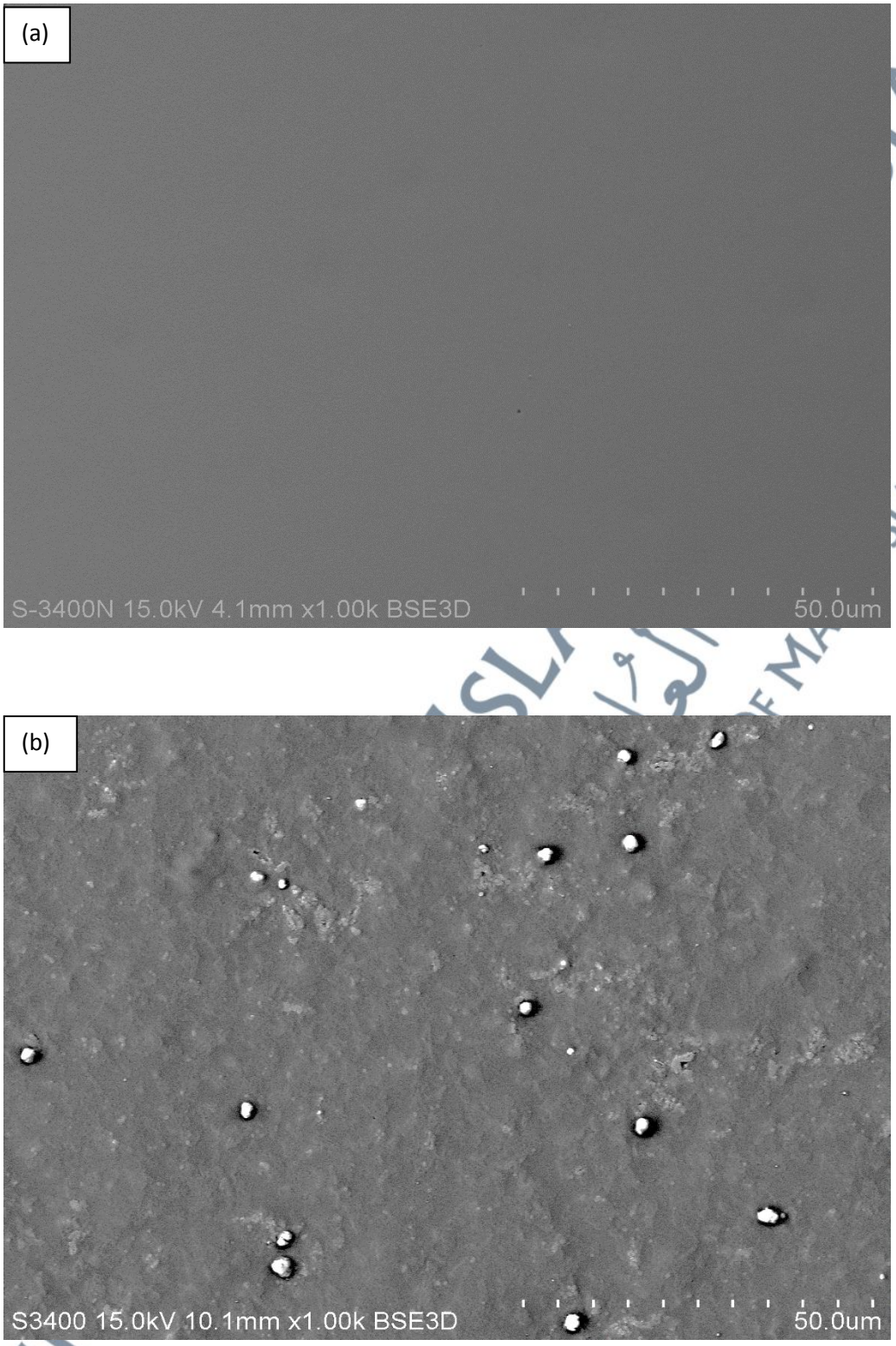

Figure 4.4: SEM images of: a) PVA:CMC thin film,

b) PVA:CMC -CRL

4.3 Characterization Using Energy Dispersive X-Ray Spectrometer (EDX)

In this study, EDX, a chemical microanalysis technique was used in conjunction with the scanning electron microscopy (SEM) technique. Analysis using EDX is important in the determination of the elemental compositions in the samples. In this study, the elemental compositions provide evidence about the entrapment of CRL in CMC, PVA and PVA:CMC thin films.

Figure 4.5 shows the EDX spectra of the supports used for immobilization (CMC, PVA and PVA:CMC) and the immobilized CRL. In all cases, gold (Au) was found to be present since gold was used to sputter coat for all samples to avoid charging when analysed under the electron beam. This is because nonconducting samples invariably need some sort of treatment before they can be examined and analyzed under optimal conditions in electron-beam instruments that rely on an emitted signal to provide information. The treatment was also necessary to eliminate or reduce the electric charge that builds up rapidly in a nonconducting specimen when it is scanned by a beam of high-energy electrons (Goldstein et al., 1992). From the EDX spectra, it is also contains carbon (20% - 50%) and oxygen (20% - 50%) due to their organic nature and common elements.

CMC thin-film, however, contains a trace amount of sodium (8.06%), as shown in Figure 4.5(a), which may have originated from the sodium hydroxide added to crude cellulose during alkalization and etherification. Besides carbon, oxygen and sodium, EDX spectra of CMC-CRL (Figure 4.5b) also showed the existence of calcium (0.3%) as evidence of the presence of CRL within the thin film. A similar observation was

obtained for the EDX spectra of PVA thin film (Figure 4.5c), it was found to contain 47.76 % of carbon and oxygen and also 0.40 % of sodium. For PVA-CRL (Figure 4.5d), it contains with 5.27% of calcium. For PVA:CMC-CRL (Figure 4.5f) spectra, the sample was found to contain 12.68% sulphur, in addition to the elements mentioned above (carbon, oxygen, sodium and calcium).

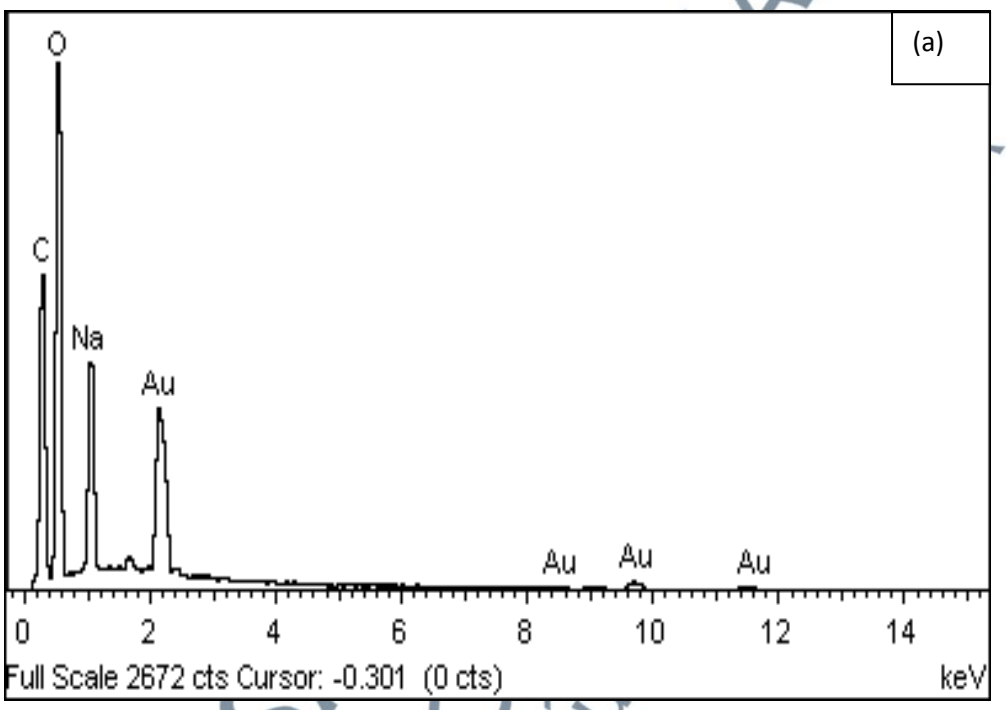

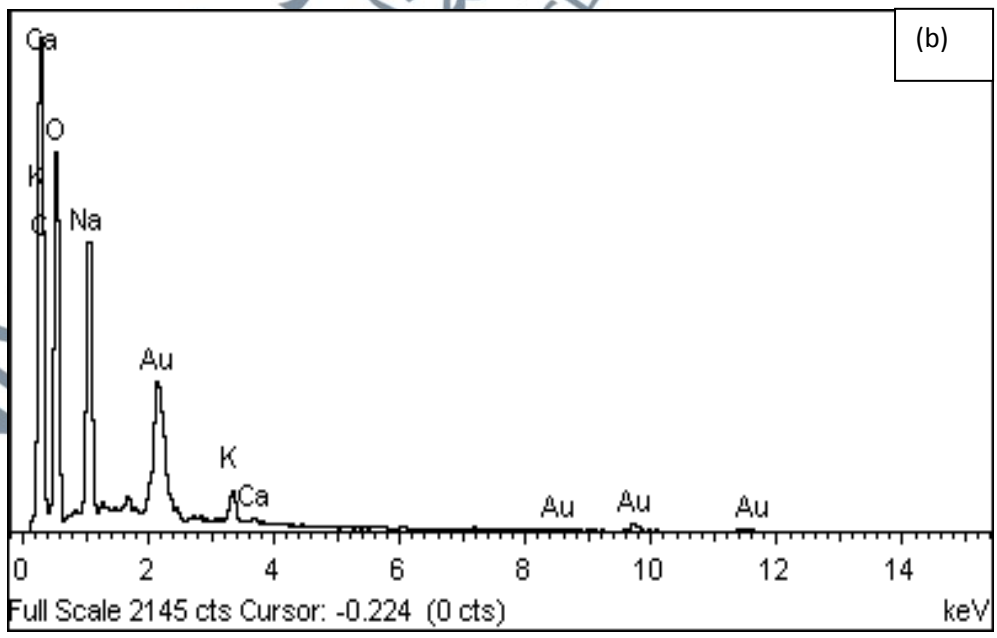

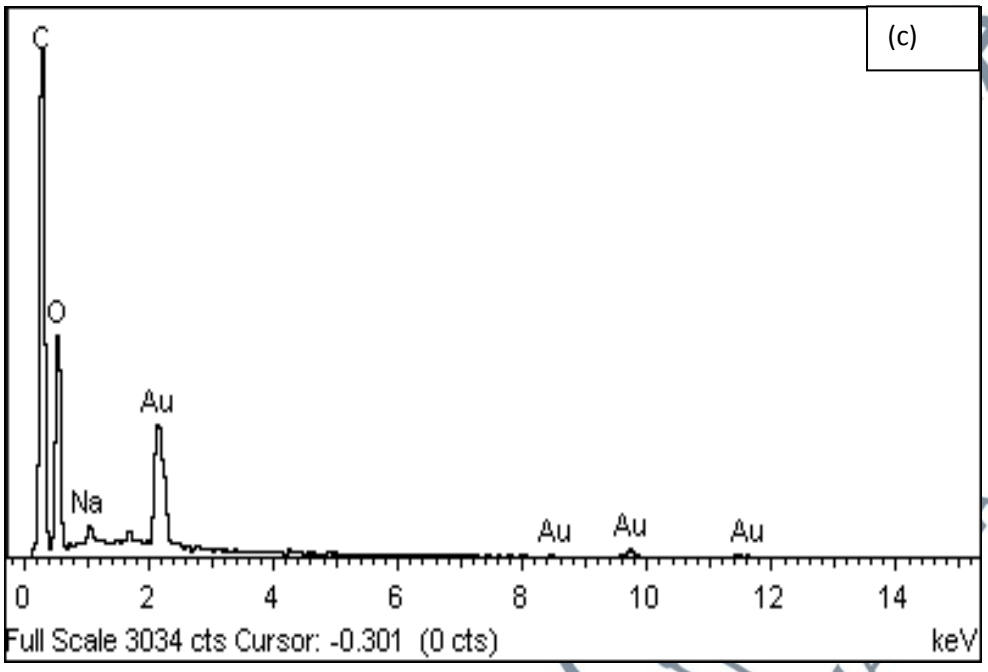
(c)
C
O
Na
Au
Au
Au
Au
0
2
4
6
8
10
12
14
Full Scale 3034 cts Cursor: -0.301 (0 cts)
keV

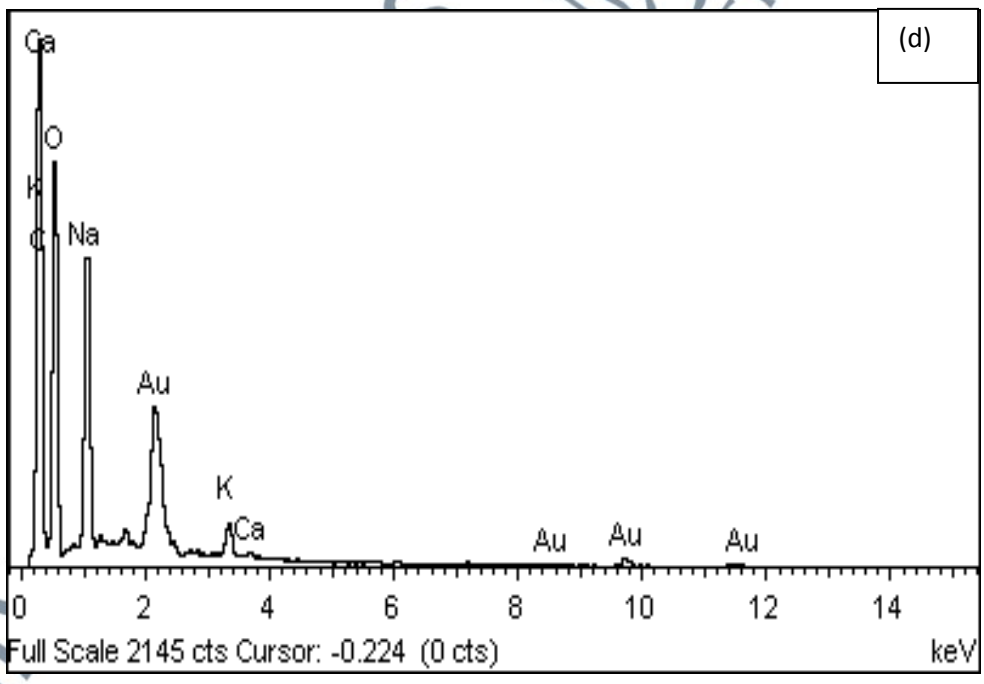
(d)
Ca
O
K
C
Na
Au
K
Ca
Au
Au
Au
0
2
4
6
8
10
12
14
Full Scale 2145 cts Cursor: -0.224 (0 cts)
keV

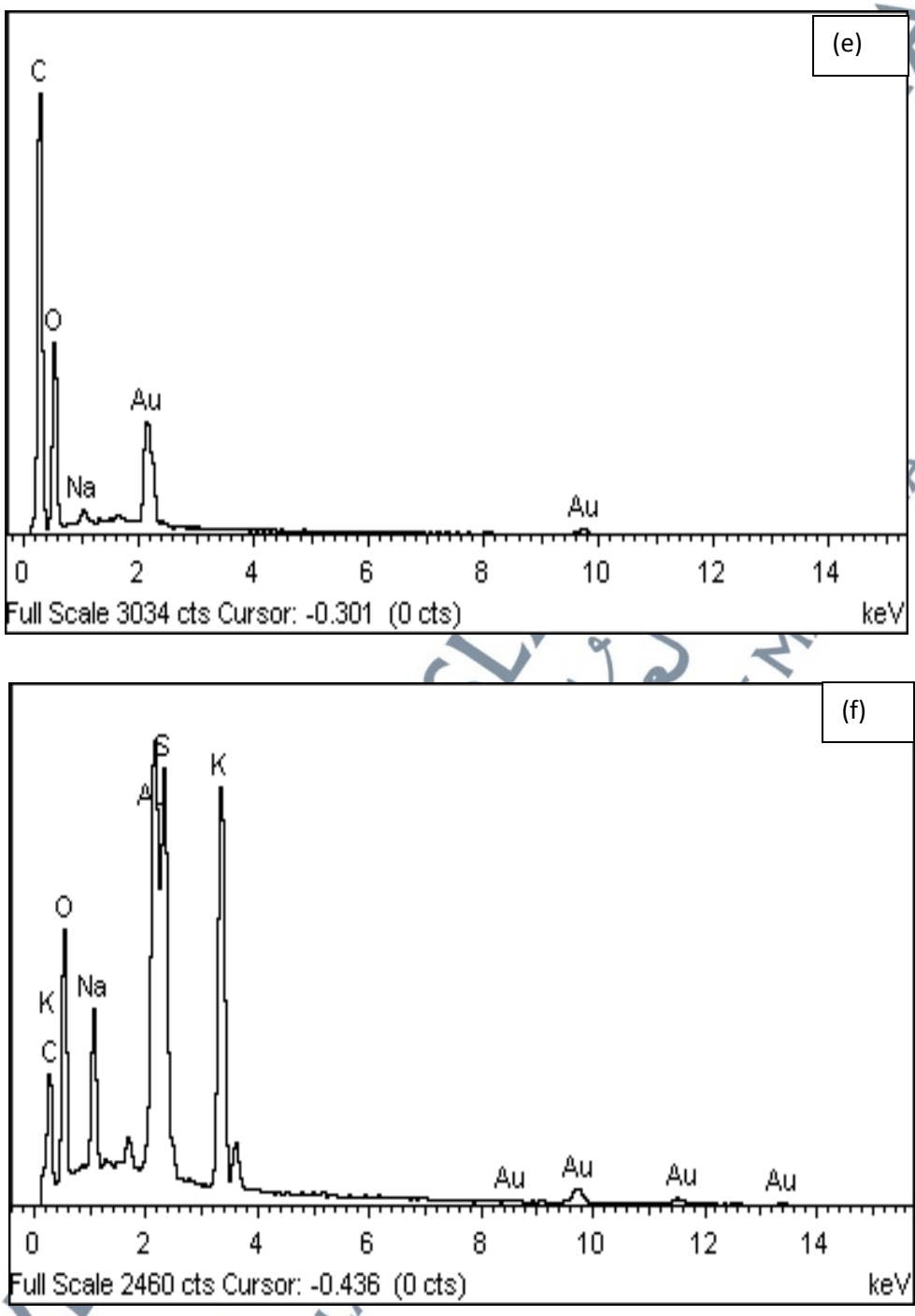

Figure 4.5: EDX image of a) CMC thin film, b) CMC-CRL, c) PVA thin film, d) PVA-CRL, e) PVA:CMC thin film , f) PVA:CMC-CRL

Table 4.1: EDX elemental analysis of free CRL of support and immobilized CRL

Types	Elements (Weight %)							
	C	K	O	P	Ca	Na	Mg	S
CMC thim film	28.37	nd	43.37	nd	nd	8.06	nd	nd
PVA thin film	47.76	nd	47.76	nd	nd	0.40	nd	nd
PVA:CMC thin film	48.96	nd	31.39	nd	nd	0.64	nd	nd
CMC-CRL	46.85	1.46	33.29	nd	0.30	8.38	nd	nd
PVA-CRL	23.43	4.07	21.38	7.46	5.27	0.80	1.31	nd
PVA:CMC -CRL	9.62	17.84	21.88	nd	nd	3.96	nd	12.68

4.4 Cross-Sectional Scanning Electron Microscopy (SEM) of Supports and Immobilized Lipases

In addition to the SEM-EDX analysis of samples, SEM was used to observe the morphological structure of the cross-sections. The method was also used to measure the thickness of the thin films.

As shown in Figures 4.6(a) and Figure 4.7(a), the cross-sectional images of CMC and PVA thin films showed a uniform pore distribution. Figure 4.8(a) however showed uniform pore distribution with a gradual decrease of pore sizes towards the top (surface) of the film. This is in agreement with the report by Teng et al (2018) whereby it was observed that the continuous space network porous structure of the section was formed, which indicated that the pore size gradually decreased from the top to the bottom. It was evident that the porosity decreased gradually with decreasing pore size.

More porous morphological structures of the thin films were observed for CMC, PVA and PVA:CMC thin films containing lipase, observed in Figures 4.6(b), 4.7(b) and 4.8(b). These were indications that the globular protein structures of CRL have been successfully entrapped within the supports. According to the Choo et al (2016), the results from FESEM analysis justified that low loading levels of TOCNs were dispersed uniformly and homogeneously in the PVA-CS blend matrix.

The thicknesses of the CMC and PVA:CMC thin films were found to decrease from 45.7 µm to 28.8 µm and 48.2 µm to 21.7 µm, respectively, after immobilization of lipase. The reduction of thickness after CRL was entrapped within the thin films was

due to densification after the introduction of CRL to the support similarly reported by Wang et al (2015). In their research, they illustrated the thickness is dependence on refractive index as deposited ALD-Al_2O_3 films revealed by SE fitting. It can be found that with increasing thickness, the refractive index of Al_2O_3 is decreasing. It is also indicated that the thickness dependence of the refractive index for Al_2O_3 films reversed and shows regular evolution rule after annealing. The thickness of the SiO_2 layer slightly increased after annealing. The Al_2O_3 film went through a densification process after annealing. PVA, however, showed an increase in the thickness of the films from 31.8 µm to 33.5 µm after the introduction of lipase. Generally, the film will be under stress state after it is deposited. The reverse of changing trend may be contributed from two reasons caused by the annealing process: stress release and phase transition (Krautheim et al., 2005). In general, all cross-sectional images revealed no visible cracks, good adhesion with no interpenetration of the thin films.

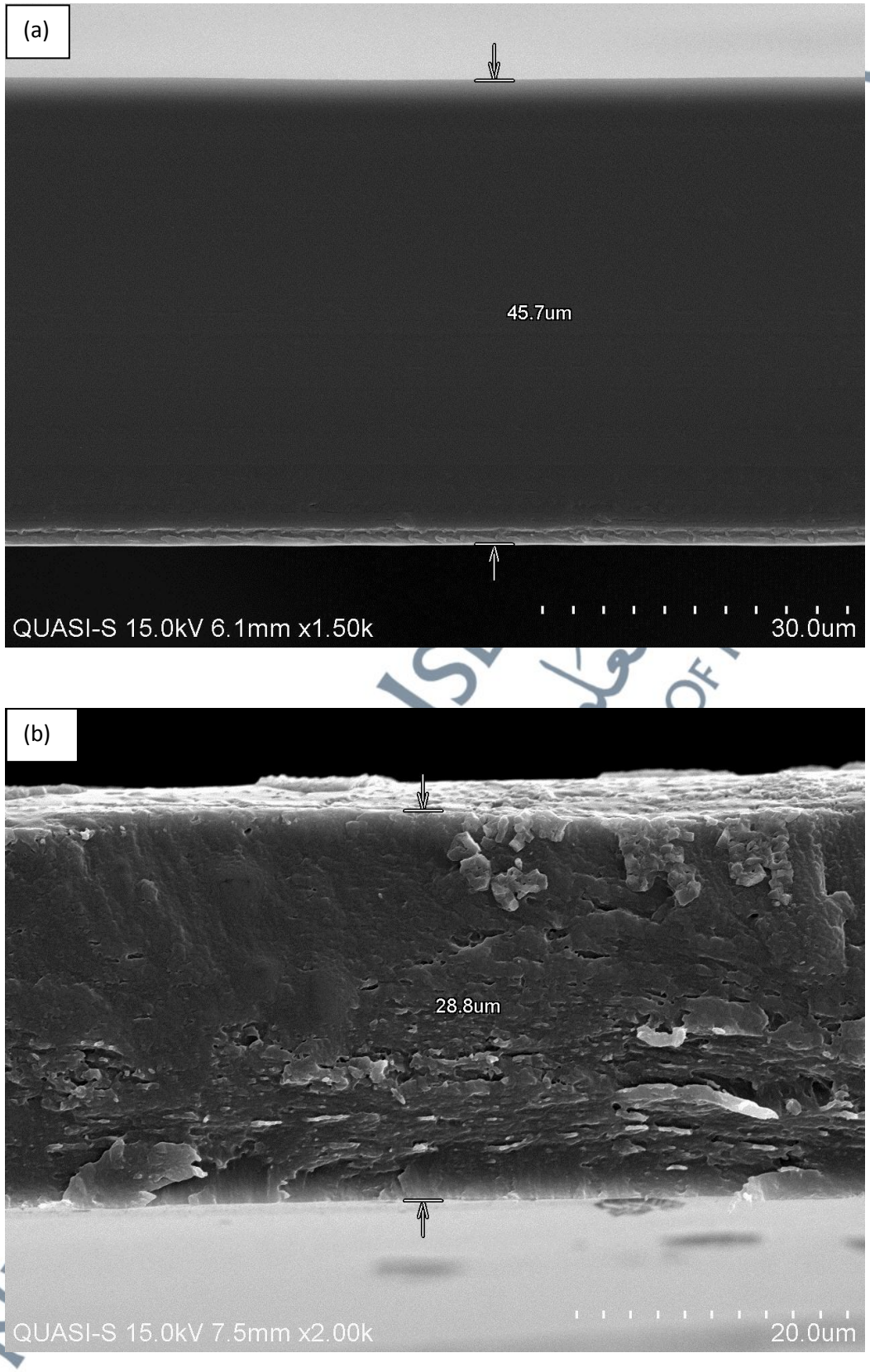

Figure 4.6 : SEM cross-sectional images of (a) CMC thin film (1500x magnifications), and (b) CMC-CRL (2000x magnifications)

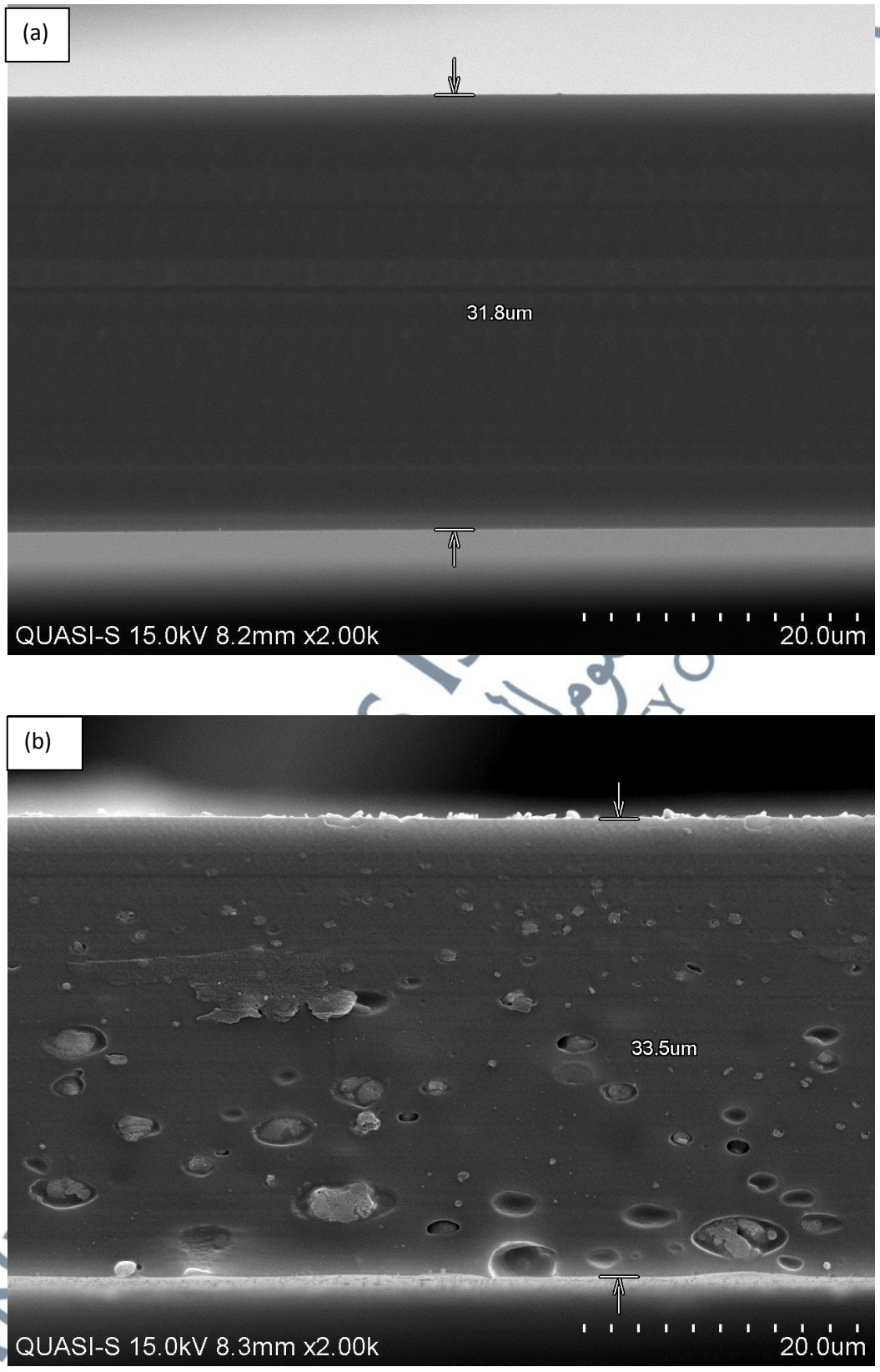

Figure 4.7: SEM cross-sectional images of (a) PVA thin film (2000x magnifications), and (b) PVA-CRL (2000x magnifications)

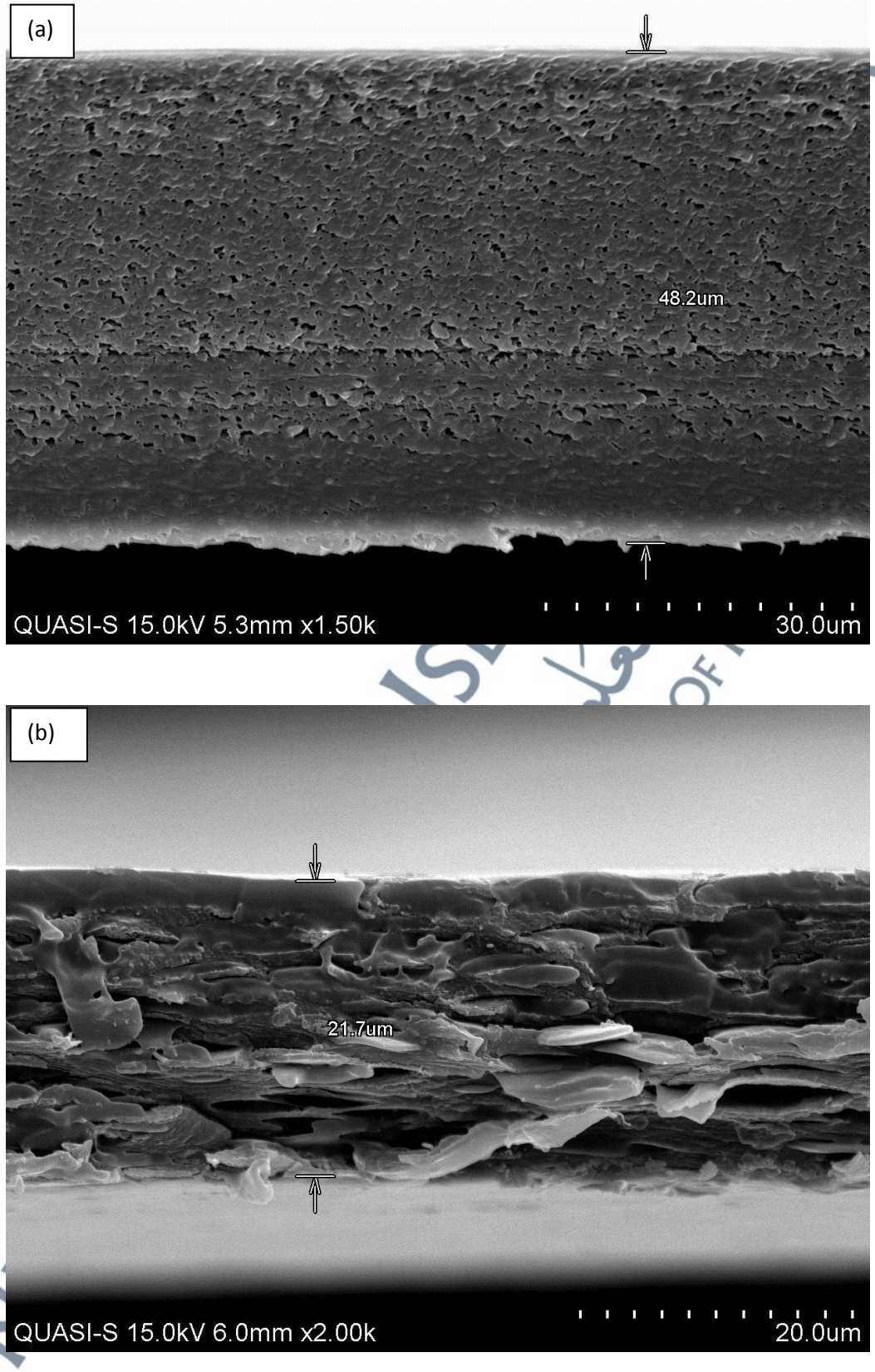

Figure 4.8: SEM cross-sectional images of (a) PVA:CMC thin film (1500x magnifications), and (b) PVA:CMC-CRL (2000x magnifications)

4.5 Characterization Using X-Ray Diffractometer (XRD)

In order to determine the crystallinity and amorphous behaviour of the polymeric materials (CMC, PVA and PVA:CMC), the characterizations has been carried out using X-Ray Diffractometer (Bruker AXS, Germany). This instrument is important in solid-state materials characterization which provides information on the crystal structural behaviour of the polymer material (Ibrahim et al., 2011).

In this study, patterns from the analysis using XRD were obtained via graphical analysis of data using DIFFRAC^{plus} Software (Bruker AXS, Germany), expressed as basal or d-spacing, which indicates the distance between similar atomic planes in the sample (the interatomic spacing) or the distance between similar faces of adjacent layers within the sample, measured in Angstroms (Å).

The XRD patterns and d-spacing of the CMC, PVA and CMC:PVA polymers with and without *Candida rugosa* lipase (CRL) are as shown in Figures 4.9, 4.10 and 4.11, respectively. In Figure 4.9, the XRD patterns of CMC exhibited a broad peak at 2θ angle position between 20^o – 30^o, indicating the presence of the amorphous region in the polymer. To be exact, the d-spacing value for CMC was 4.32 Å, at $2\theta = 20.56^o$ while the CMC-CRL showed a d-spacing value of 4.14 Å, at $2\theta = 21.42^o$. It is obvious that the d-spacing values decreased when CRL was incorporated (immobilized) within the CMC polymer as reported by Emam et al., (2019). In their study of XRD pattern, CMC was observable with two intense diffraction peaks at $2\theta = 9.6^o$ and 20.6^o which are characteristic of CMC.

In Figure 4.10, XRD patterns of PVA and PVA-CRL however showed narrow peaks which indicated the presence of crystalline regions in the samples. The broad peak between $2\theta = 40.1^{o}$ can be described in the amorphous phase in PVA. From the previous research done by Aziz et al (2017), it can be seen that the XRD pattern of pure PVA shows a peak around $2\theta = 20^{o}$ corresponding to the semi-crystalline nature of pure PVA. The existence of OH groups along the main chain of PVA is enough to provide strong intermolecular and intra molecular hydrogen bonding in PVA and at the $2\theta = 40.7^{o}$, the broad peak pattern can be ascribed as amorphous region in PVA. The *d*-spacing value for PVA was 4.65 Å, at $2\theta = 19.05^{o}$ while PVA-CRL showed a similar decrease in *d*-spacing value of 4.63 Å, at $2\theta = 19.16^{o}$.

Similar observations were obtained in Figure 4.11 for PVA:CMC thin film with and without the presence of CRL. Interestingly, when PVA is blend with CMC, the crystalline behavior of PVA dominated the mixture. This could be due to the amount of PVA which was (1:1) to CMC. A similar finding was obtained by Morsi et al, (2019) where the diffraction peak at 19.70^{o} in the XRD pattern of PVA:CMC blend indicates its semicrystalline nature because of the existence of PVA with content (70%wt) within the blend structure. The PVA:CMC thin film showed a *d*-spacing value of 4.62 Å at $2\theta = 19.22^{o}$. This value, however, decreased to 4.14 Å, at $2\theta = 21.42^{o}$ when CRL was incorporated into the polymer. The differences in *d*-spacing of thin films before and after immobilization of CRL are shown in Table 4.2.

The reasons of decreasing d-spacing of CMC, PVA and PVA:CMC after immobilization of CRL is due to the intensity was significantly decreased, which was mainly due to the dense accumulation of enzymes (CRL) in the pore, reducing the

electron density between the supports wall and the pore as reported by Wang et al (2019). In their research of Mesoforous Carbon-Based Enzymes Biocatalyst for Aquatic Recalcitrant Pollution Treatment, the XRD patterns change greatly after lysozyme was loaded and none of the two characteristic peaks appeared, and the intensity was significantly decreased, which was mainly due to the dense accumulation of lysozyme in the pore, reducing the electron density between the carbon wall and the pore.

Table 4.2: Basal spacing of thin films before and after immobilization of CRL

Types of Thin films	***d*-spacing (Å)**	
	Before CRL immobilization	After CRL immobilization
CMC	4.32	4.14
PVA	4.65	4.63
PVA:CMC	4.62	4.14

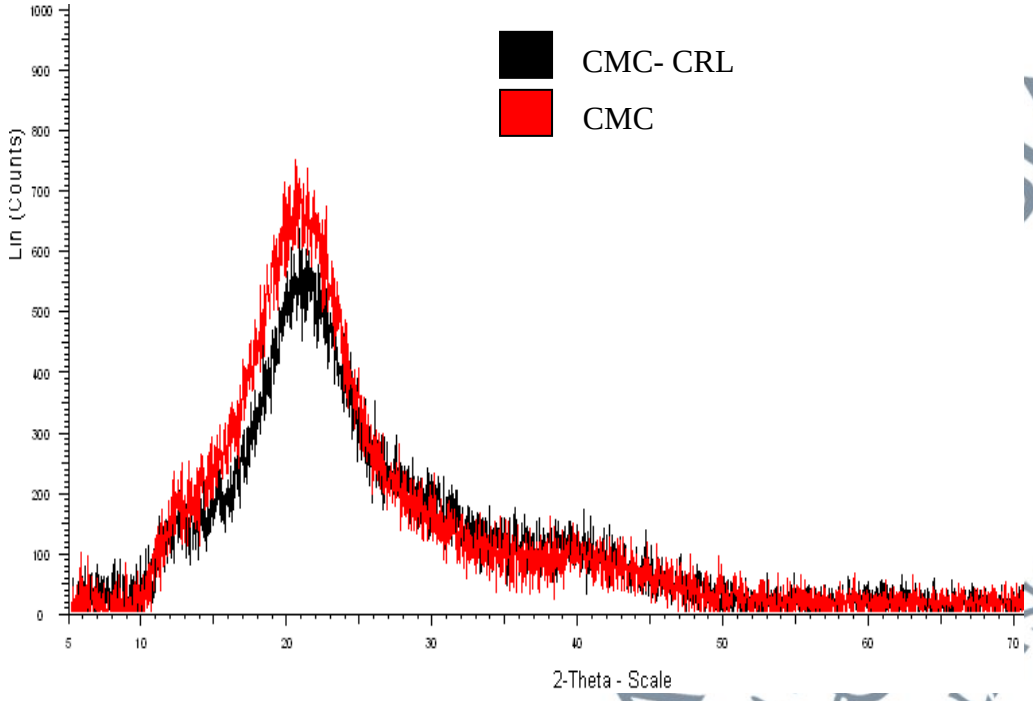

Figure 4.9: XRD patterns of CMC thin film and CMC-CRL

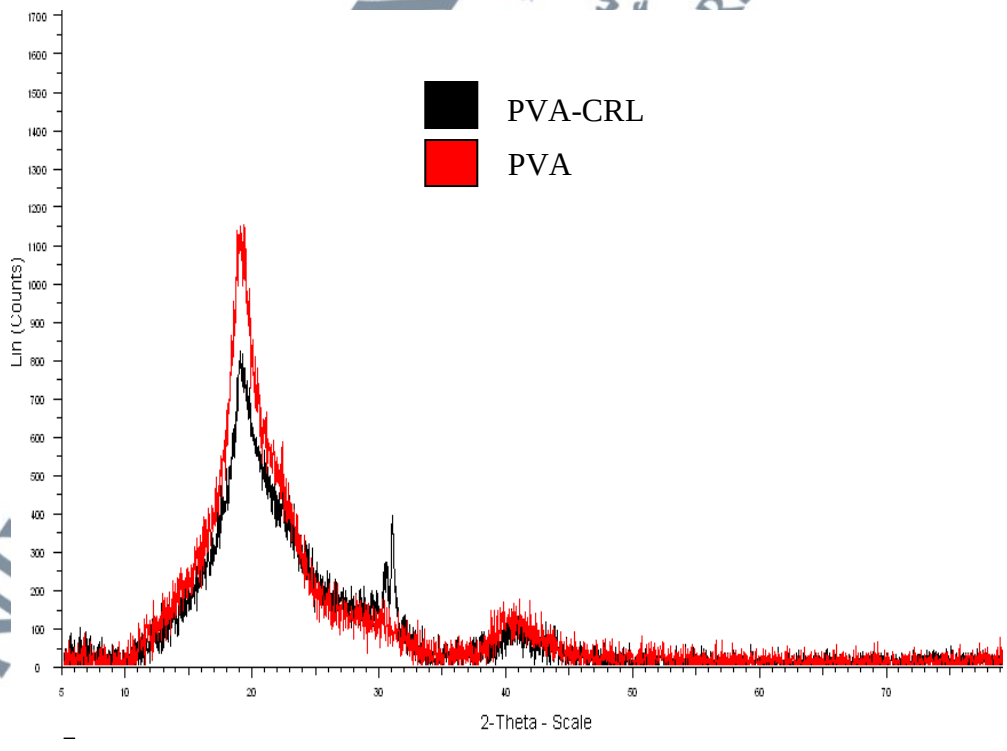

Figure 4.10: XRD patterns of PVA thin film and PVA-CRL

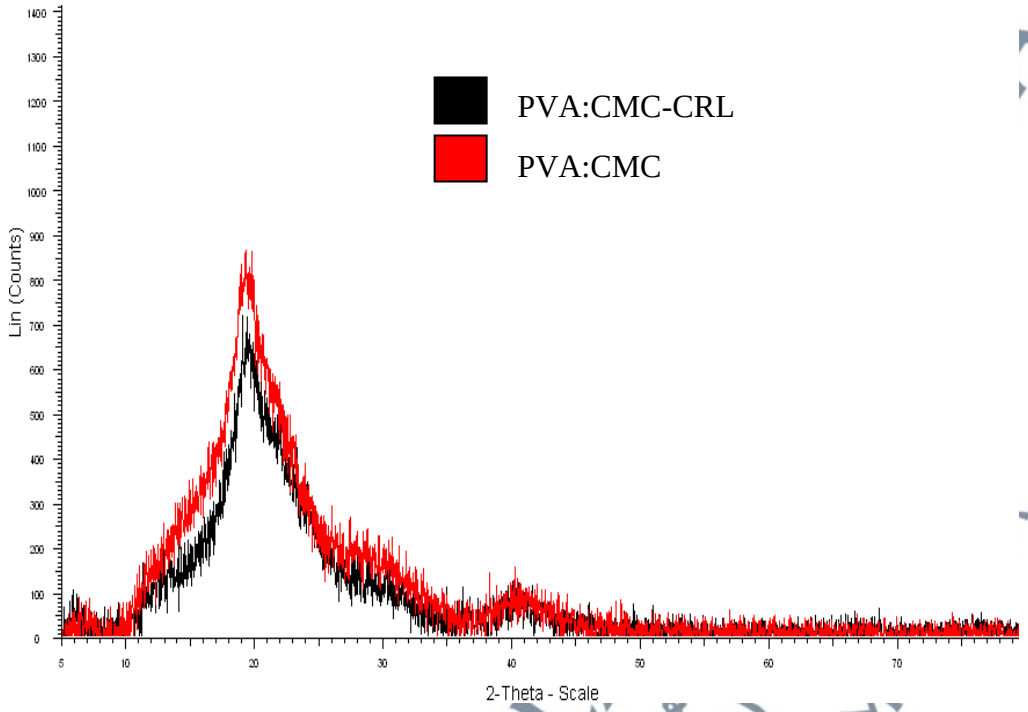

Figure 4.11: XRD spectra of PVA:CMC thin film and immobilized PVA:CMC-CRL

4.6 Characterization Using Fourier Transform Infrared (FTIR) Spectrometer

In order to characterize the physico-chemical behaviour of the support materials before and after immobilization of CRL, Fourier Transform Infrared (FTIR) spectrometer was used. Analysis using FTIR spectrometer is also useful in the identification of functional groups presence on the samples.

In general, all samples were found to contain carboxyl and methyl groups indicated by the presence of bands at 1618 cm^{-1} and 1426 cm^{-1} wavenumber, respectively. Broad peaks from 3300 to 3400 cm^{-1} region were attributed to the stretching of O-H groups, while the peaks present between 2800 cm^{-1} and 2900 cm^{-1} were attributed to the stretching of C-H groups.

Based on Figure 4.12, the peaks at wavenumber 1314 cm^{-1} indicated the presence of methyl and hydroxyl groups while peaks at 1548 cm^{-1} indicated the presence of the carboxyl group in CMC. A significant broad-band between 2800 cm^{-1} and 3630 cm^{-1} was due to the stretching of hydroxyl (OH) group in the sample, while the band present at 2942 cm^{-1} was due to the presence of alkyl (C-H) stretching. Finally, the band at 1076 cm^{-1} was due to the presence of CH-O-CH stretching. All of these peaks and bands are correlated to the functional groups present in CMC, which has a chemical formula of $C_6H_7O_2(OH)_2CH_2COONa$.

Figure 4.13 on the other hand shows the FTIR spectra of PVA. All major peaks present were found to be related to hydroxyl and acetate groups. Broad-bands observed between 3550-3200 cm^{-1} indicated the presence of O-H stretching, while bands observed between 2840 cm^{-1} and 3000 cm^{-1} refer to the stretching from alkyl (C-H) groups, which correlates to the functional groups present in PVA.

Almost similar bands as in Figure 4.12 and Figure 4.13 were found in Figure 4.14, which is the FTIR spectra of PVA:CMC. A band observed at 2924 cm^{-1} wavenumber was due to the presence of C–H stretching, found in the $-CH_2$ group of the PVA:CMC blend. A band due to the stretching of glucose ring in the CMC structure, was also found to appear at 1600 cm^{-1}. In addition, the FTIR spectra in Figure 4.14 also showed the existence of bands in the region between 1350 – 1450 cm^{-1} which were due to the symmetrical deformations of CH_2 and COH groups in PVA. The bands indicating the presence of alcoholic $–CH_2OH$ stretching and CH_2 twisting and vibration were also observed at 1078 cm^{-1} and 1021 cm^{-1}, respectively.

The spectrum of CRL is typical for a protein, with the most prominent band at 1636 cm^{-1} (amide I) that originates from –C═O stretching and –NH bending vibrations and the band at 1123 cm^{-1} from the carbohydrate moiety of the enzyme. The appearance of some peaks and the disappearance of others in the spectrum of the immobilized enzyme confirmed successful (Prlainovic et al., 2016). All the spectra can be summarized in Table 4.2.

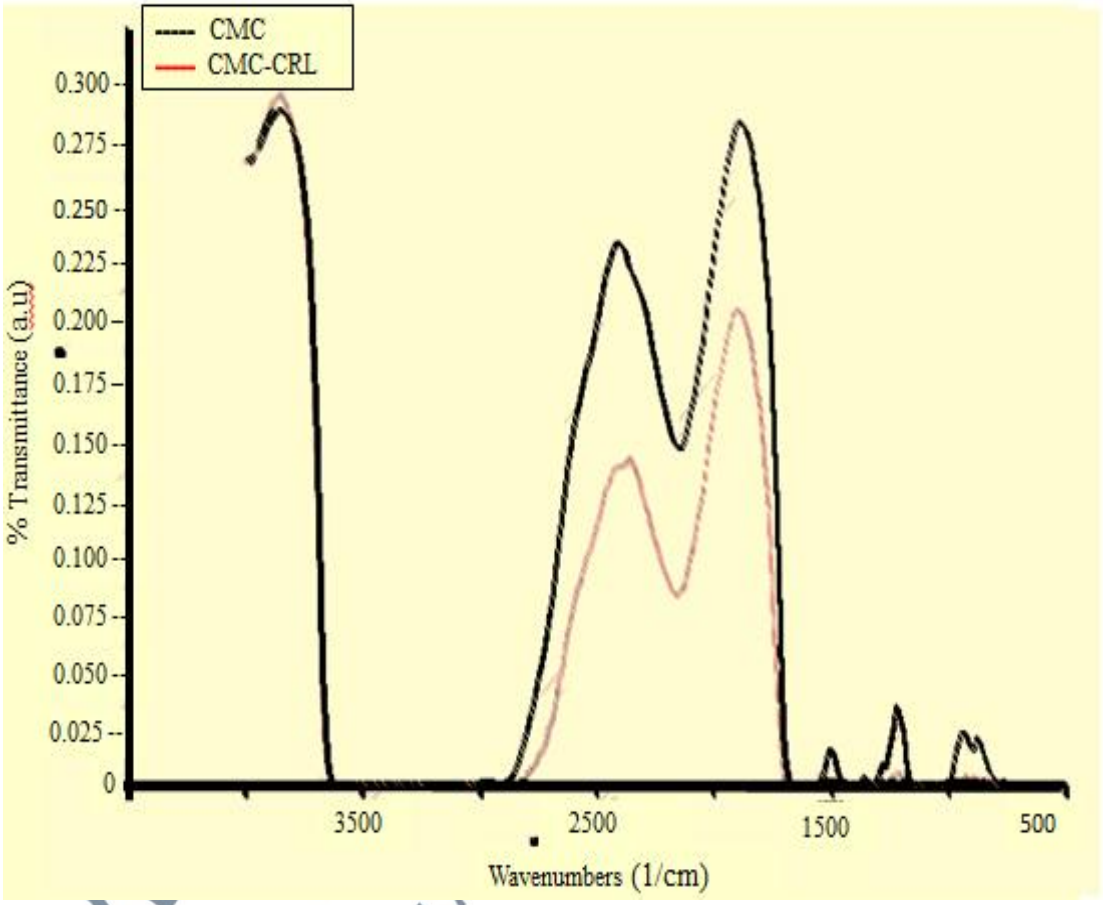

Figure 4.12 : FTIR Spectra of CMC thin film and CMC-CRL

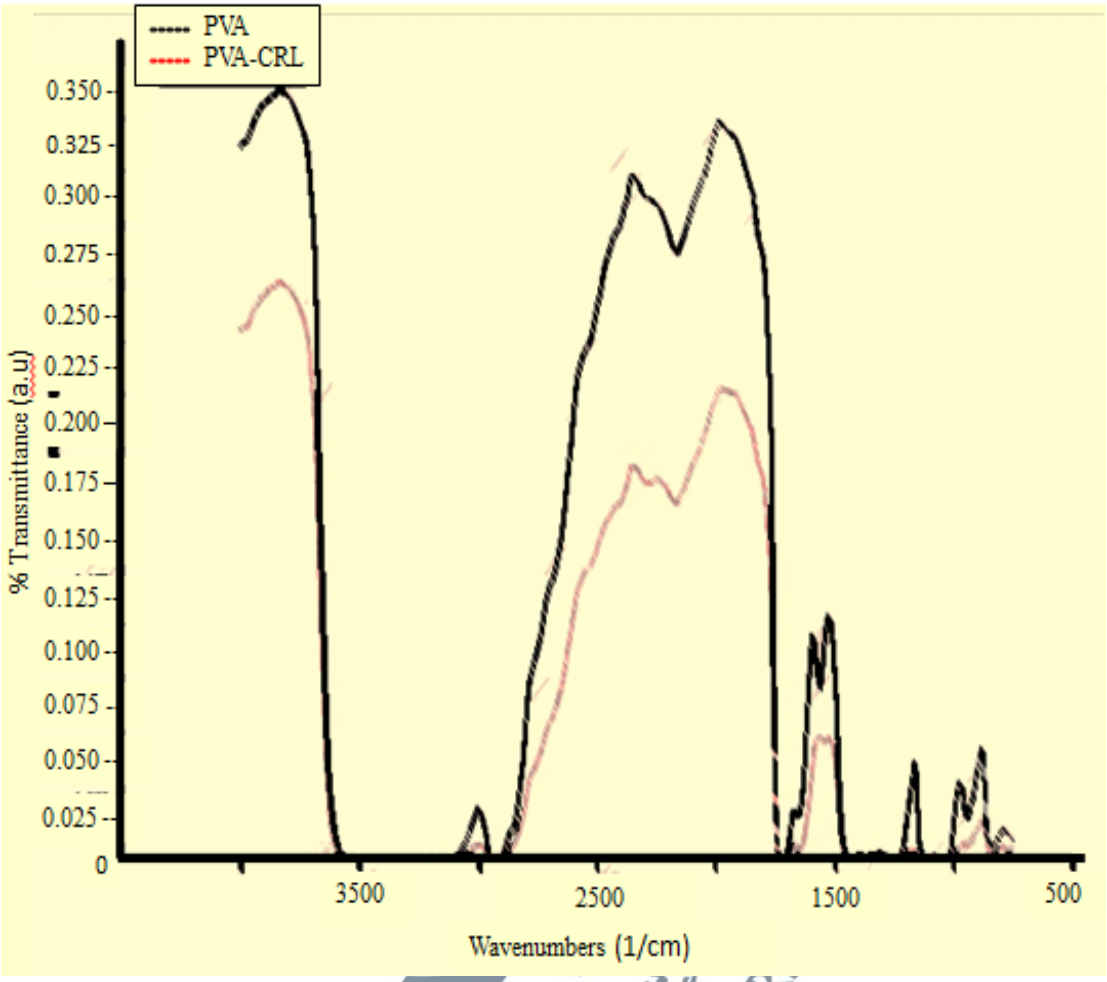

Figure 4.13 : FTIR Spectrum of PVA thin film and PVA-CRL

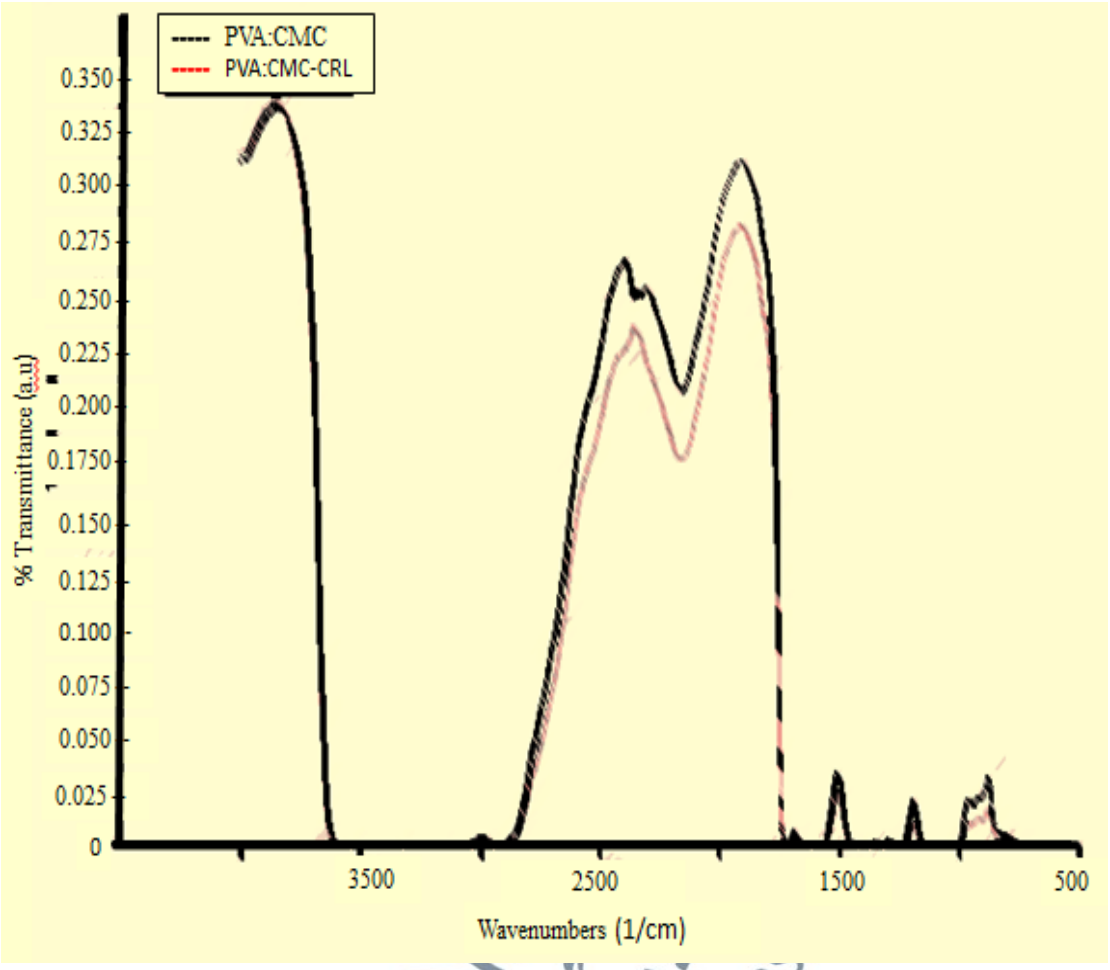

Figure 4.14 : FTIR Spectrum of PVA:CMC thin film and PVA:CMC-CRL

Table 4.3: Summary of FTIR analysis result

Wavenumber (cm^{-1})	Assignments
1021	$–CH_2$ twisting and vibration
1076	CH-O-CH stretching
1078	Alcoholic $–CH_2OH$ stretching
1314	methyl and hydroxyl group
1350 - 1450	Symmetrical deformations of CH_2 and COH group
1548	carboxyl group in CMC
1600	Stretching of glucose ring in CMC
2924	Alkyl(C-H) stretching
2840 - 3000	Stretching of alkyl (C –H) group
2800 - 3630	the hydroxyl (O-H) stretching

4.7 Stability Assay of Native and Immobilized Lipases

4.7.1 Storage Stability

Storage stability is one of the many crucial factors to be considered when using immobilized CRL. It is, in fact, a measure of the ability of the immobilized enzyme to maintain its stability and activity even after 60 days of storage at different temperatures, -20 ^{o}C, 0 ^{o}C, 4 ^{o}C and room temperature (27 ^{o}C).

In the determination of lipase activities through esterification between oleic acid and butanol, it was found that the activity of CRL decreased naturally as storage temperatures were increased. However, the decrease in activities of immobilized lipases was gradual and not drastic, as compared to the native CRL.

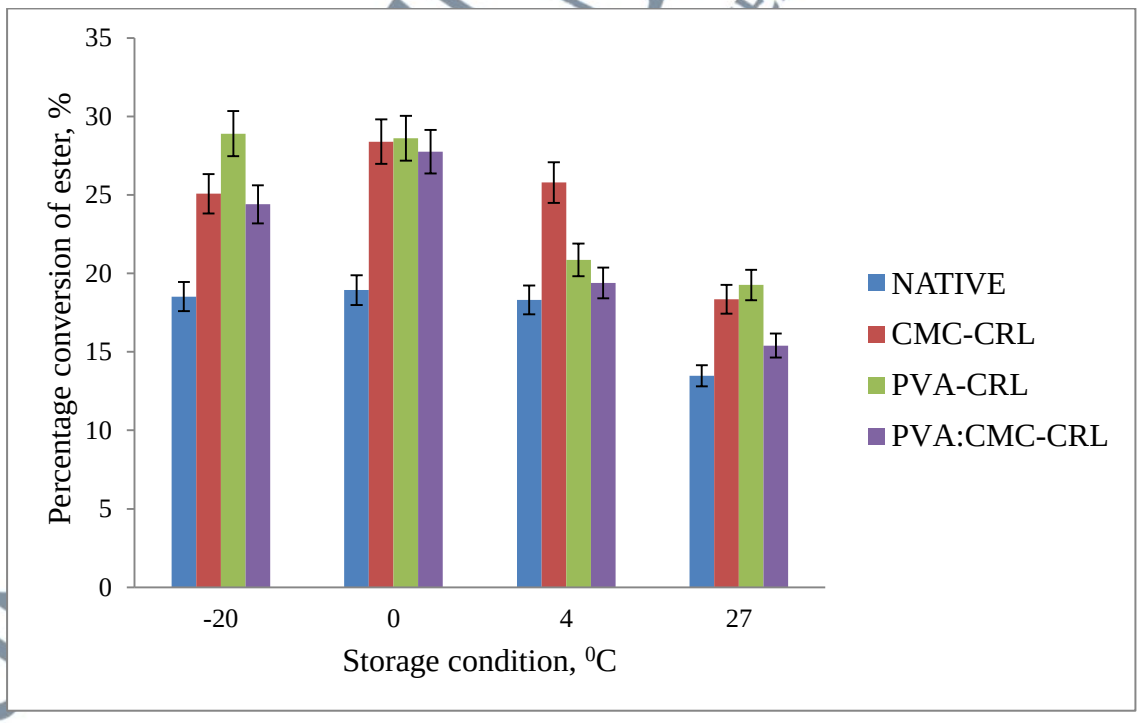

Figure 4.15 : Percentage conversion of ester (%) vs storage condition ^{0}C for native CRL and immobilized CRL.

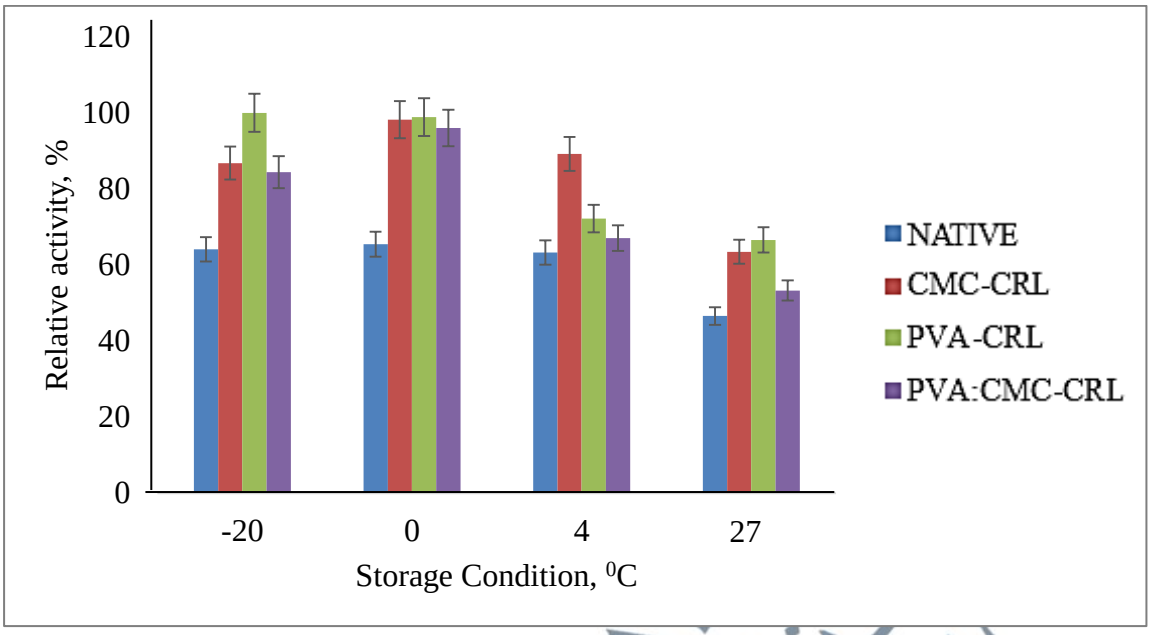

Figure 4.16 : Relative activity (%) vs storage condition ^{0}C for native CRL and immobilized CRL.

As shown in Figure 4.15 and 4.16, all immobilized lipases were found to retain higher activities than native lipase after 60 days of storage at various temperatures. PVA-CRL was found to be more stable and retained 100% of its activity after 60 days of storage at low temperature (0 ^{o}C). At -20 ^{o}C, the native lipase activity was repeated at 65%. The high stability (100%) at low temperature (-20 ^{o}C) was also shown by PVA-CRL.

CMC and PVA:CMC immobilized lipases however, retained 86.8% and 84.4% activities after 60 days of storage at -20 ^{o}C, respectively. Furthermore, it can be observed that, the immobilized lipases obtained more than 70% catalytic activity when stored at 0 ^{o}C while native lipase has decreased to 60% of its catalytic activity over a period of 60 days. Besides that, the stability of the immobilized lipases at 4 ^{o}C is almost 65% which was still high compared to the native enzyme which was 40% at

the same storage temperature. According to Mohamad et al. (2015), the stability achieved was referred to the multiple attachments of the enzyme to the support, preventing any intermolecular process such as proteolysis and aggregation, therefore creating a more rigid enzyme molecule.

4.7.2 Reusability (Operational Stability)

The reusability of enzyme constitutes should be the main aim of the immobilization process. It is an important measure for the economic viability of a biosynthetic process and enzyme ability to be repeatedly used in batch reactors. Moreover, the use of immobilized enzyme should permit to greatly simplify the design of a reactor and the control of a reaction. Thus, the idea of enzyme reusability implicitly means that the stability of the enzyme preparation should be high and immobilization is efficient enough to permit this reuse (Mateo et al., 2007).

To assess the reusability of immobilized CRL systems, hydrolysis yields were examined during 9 successive 24 h hydrolysis reactions. From the study (Figure 4.17), it is evident that relative activities gradually decreased from the first (100%) until the fifth cycle (>50%), for all CMC-CRL, PVA-CRL and PVA:CMC-CRL used. Among the immobilized enzymes, PVA-CRL is the most stable compared to the other immobilized enzymes. CMC-CRL, PVA-CRL and PVA:CMC-CRL were possessed > 60% of its enzymatic activity in the 4th cycle regardless of which immobilization of CRL were used. However, for the 5th cycle, the enzyme activities of CMC-CRL, PVA-CRL and PVA:CMC-CRL have decreased to >50%. Decreased in immobilization enzyme activities was due to entrapment of the CRL, also limits

substrate accessibility if the substrate cannot easily diffuse into the porous support, which can also lower levels of hydrolysis. The relatively low rates of enzyme hydrolysis observed were expected as we used carboxymethyl cellulose for these experiments, which is composed of cellulose that is highly ordered and more resistant to hydrolysis. This is in agreement with the study done by Ikeda et al (2015). In their research, hydrolysis yields were examined during 9 successive 24 h hydrolysis reactions. Immobilized C1 possessed >40% of its enzymatic activity in the 6th cycle regardless of which immobilization silica was used. Conversely, C2 possessed only 23% and 29% of its activity in the 6th cycle when immobilized on S1 and S2, respectively. However, C2S1 possessed 54% of its enzyme activity in the 4th cycle and that of C2S2 was 50% in the 5th cycle. During the 4th cycle, C1S1 and C1S2 maintained 66% and 77% of their activity, respectively. Taken together, using our immobilization system, C1 and C2 maintained ≥ 50% of their activity for at least 4 cycles.

Interestingly, all of the immobilized lipases showed stabilized activities (50%) after the fifth cycle. These stabilized activities could be due to the bioimprinting process where lipase suspended in reaction media (organic solvents) tend to be more rigid as a result of increased electrostatic and hydrogen bonding interactions among the surface residues of the protein in organic solvents. According to Cao et al (2009), after several cycles of immobilized enzyme reusability, the formation of water as by-product from the esterification process became the factor that executes the bio-imprinting process. In this study, bioimprinting with substrate analogues of fatty acids was systematically conducted to improve the esterification activity of Burkholderia cepacia lipase that had undergone a sol–gel immobilization procedure with methyltrimethoxysilane

(MTMS) and tetramethoxysilane (TMOS) as the precursors. The specific activity of the bioimprinted lipases was 3682.0 μmol h^{-1} mg protein, which was a 47.9- and 2.5-fold increase over the free and non-imprinted immobilized lipases, respectively. As compared to the free and non-imprinted immobilized lipases, bioimprinted lipases exhibited better thermal stability, and their activity did not change after being incubated at 60 °C for 12 h. Bioimprinted lipases were more easily affected by alcohol than the non-imprinted ones, whose specific activity could be markedly enhanced by ethanol, isopropanol and n-butanol by factors of 1.23-, 1.28- and 1.12-fold, respectively. The reasons for the improvement of imprinted enzyme activity are also discussed based on the surface structure, specific surface area and average pore diameter of the silane particles (Cao et al., 2009).

To date, bioimprinting has become an alternative process to alter selectivity and improve the activity of enzymes by pre-treating them with inhibitors or substrate analogues. This, however, has to be carefully done because the addition of water to organic solvent reaction media may strongly depress the activation of imprinting because of an increase in enzyme flexibility upon rehydration. According to Fishmen and Cogan (2006), bio-imprinting of lipases with fatty acids was shown to be a feasible, effective method for obtaining highly active enzymes in organic solvents. The increase in activity was dependent on the enzyme type, the solvent type and the imprint molecule itself. A correlation between the initial activity of caprylic acid-imprinted Candida rugosa lipase (CRL), and solvent hydrophobicity was observed. In addition, the combination of bio-imprinting with adsorption onto inert support such as celite, which; proved to be a powerful technique for obtaining even more active and stable enzyme preparations. In the case of lipase from Pseudomonas sp., the increase

in activity resulting from bio-imprinting with caprylic acid and immobilization onto celite, was 20-fold. Porcine pancreatic lipase (PPL), treated in the same manner, retained 70% of its initial activity at the end of 20 consecutive reaction cycles, compared to only 20% residual activity for the non-treated control.

The activities of immobilized lipases shown in Figure 4.17 are in correlation with the yields of butyl oleate produced by the lipases (Figure 4.18). At initial use, the CMC-CRL, PVA-CRL and PVA:CMC-CRL showed 100%, 93.7% and 92.3% of relative activity, respectively. Linear extrapolation (dotted lines) of the reusability data showed that the CMC, PVA and PVA:CMC-immobilized lipases possess half-life of 5^{th} cycles, respectively.

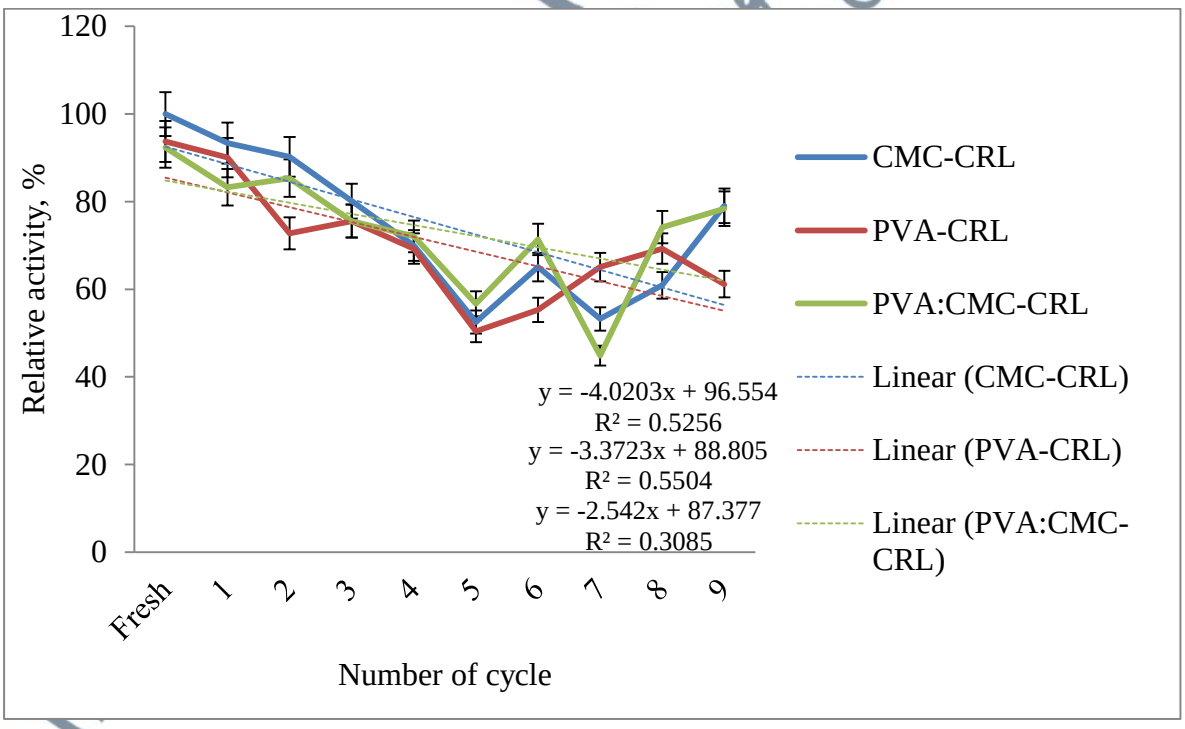

Figure 4.17: Relative activities of CMC, PVA and PVA:CMC-immobilized lipases as affected by repeated use in the esterification of butyl oleate in hexane, at 37 ^{o}C for 6 hours.

4.8 Kinetic Study of Native and Immobilized Lipases

The study of kinetics and its modelling are essential for the enzyme process scale up and reactor design in order to determine the factors that affecting the reaction rate of enzyme. In many cases lipase catalyzes reactions with acyl donor on the basis of initial rate; a model was proposed such as Ping Pong Bi Bi model was prepared with inhibition of substrate. In this study, a kinetic model was constructed on the basis of the initial rate determination by changing the concentrations of both reactants. In the esterification process of butyl oleate, free CRL and immobilized CRL into CMC and PVA supports, were carried out by maintaining one substrate (oleic acid) at constant concentration while varying the concentration of other reactants (butanol), or vice versa. For the first experiment, the initial oleic acid concentrations were varied from 2.0mmol until 10.0 mmol with the constant concentration of 2.0mmol butanol. For the second experiment, the initial butanol concentrations were varied from 2.0mmol until 10.0mmol with the constant concentration of 2.0mmol oleic acid.

4.8.1 Kinetic Modelling of Michaelis-Menten Plots

The kinetic study of the enzymatic reaction is an important parameter in order to determine the factors that influence the rate of reaction. The kinetic study can provide better insight into the reaction mechanisms of an enzyme-catalyzed reaction. The kinetics of the specific reaction can follow the specific kinetic model based on its reaction mechanism. The substrate concentration is one of the crucial factors that affect the esterification rates. Based on the experimental data, the initial rate of esterification was determined. These initial reaction velocities were then used for

identification of maximum velocity and Michaelis Menten, inhibition and dissociation constants using Ping Pong Bi Bi model.

As reported in Figure 4.18, the effects of substrate concentrations on the initial rate were indicated by representative curves at different concentration of each substrate. At the constant concentration of oleic acid, the initial reaction rates increase rapidly with increasing butanol concentrations from 2.0mmol until 10.0mmol. The reaction rate of immobilized CRL for CMC, PVA and PVA:CMC were higher than the native CRL. The immobilized CRL of CMC, PVA and PVA:CMC give more effective to the esterification process as compared to the native CRL, thus, contribute to high percentage of product. This behaviour could be proportionally related to the fact that in the immobilized system, the enzyme was not in direct contact with the alcohol as well as the microenvironment associated to the location of the hydrophobic support at the aqueous-organic interface.

Results in Figure 4.19 showed that an increase of the substrate concentrations of butanol from 2.0mmol to 10.0mmol, it promote a significant incremental on the hydrolytic activity values for both native and immobilized CRL. Similarly, the graph also illustrated higher reaction in immobilized CRL in comparison with the native CRL. The enzymatic reaction follows the Michaelis-Menten equation and no product inhibition was observed due to their ability to retain activity in such high oleic acid concentrations. From the results described above, it can be evidenced that all the reactions followed a Michaelis Menten kinetic with or without substrate inhibition. All of the calculations of reaction rate can be obtained by using the formula in APPENDIX G.

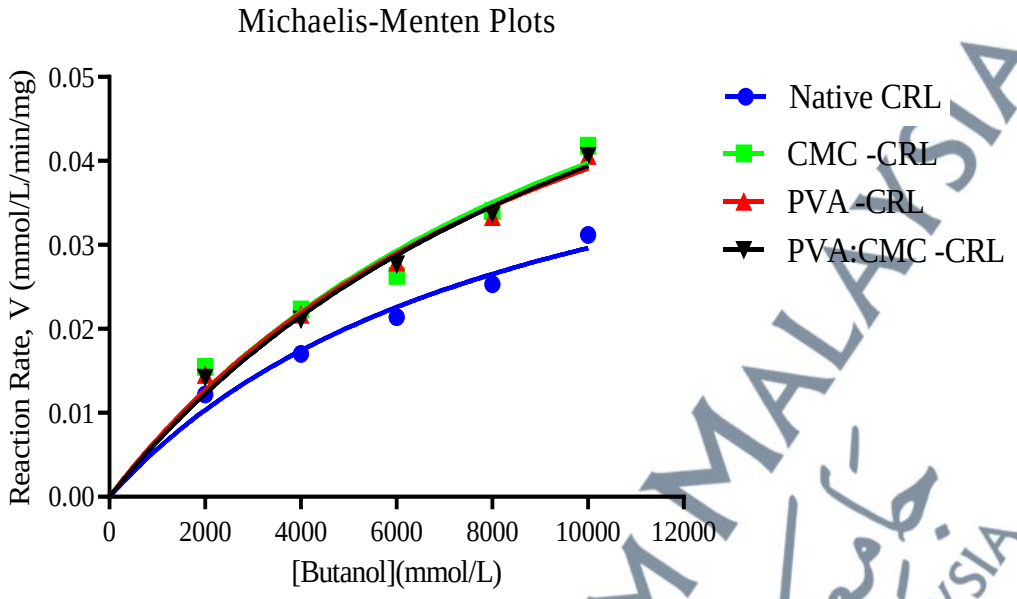

Figure 4.18: Michaelis Menten plots on the reaction rates of butyl oleate synthesis at various concentration of butanol for CRL-CMC, CRL-PVA and CRL-PVA:CMC.

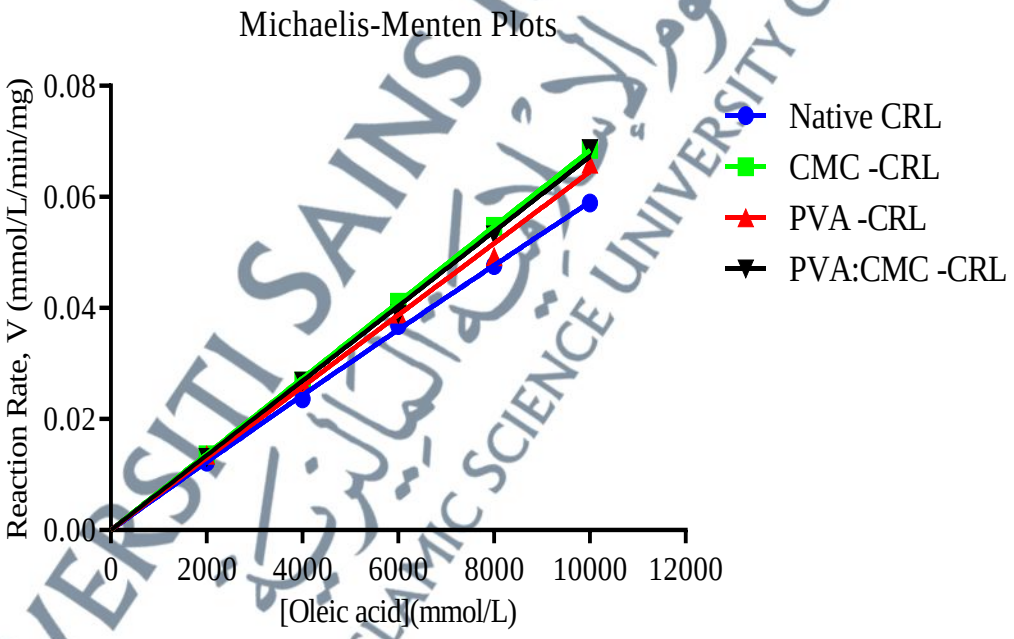

Figure 4.19: Michaelis Menten plots on the reaction rates of butyl oleate synthesis at various concentration of oleic acid for Native CRL, CMC-CRL, PVA-CRL PVA:CMC-CRL.

4.8.2 Determination of Kinetic Constants (Lineweaver- Burk Plot)

Figures 4.20 and 4.21 illustrated Lineweaver – burk (double reciprocal) plots of initial rate versus either the concentrations of oleic acid or butanol. The exact mechanism of enzymatic reactions can be obtained from Lineweaver- Burk double reciprocal plots. The Lineweaver Burk was designed by taking reciprocal of the initial rate and different concentration of butanol (Badgujar et al., 2014). The Lineweaver Burk double reciprocal plot is based on the rearrangement of the Michaelis – Menten equation into a linear form and the inverse of initial rate (V_i) is plotted against the inverse of the initial concentration of the reacting species (Yadav & Devi, 2004). When there is no inhibition, then a Ping Pong Bi Bi mechanism, the ratio of the rate of reaction at a given concentration of A and B to the maximum rate is given by;

$$\frac{V_i}{V_{max}} = \frac{[A][B]}{K_{m(A)}[B] + K_{m(B)}[A] + [A][B]} \quad (4.1)$$

and if there is inhibition by B;

$$\frac{V_i}{V_{max}} = \frac{[A][B]}{K_{m(A)}[B]\,(1+ [B] / K_{1B}) + K_{m(B)}[A] + [A][B]} \quad (4.2)$$

the inhibition by B can be established as follows: When [A] is varied, the equation is

$$\frac{V_i}{V_{max}} = \frac{[A]}{K_{m(A)}\,(1+ [B] / K_{1B}) + [A](1 + K_{m(B)}/[B])} \quad (4.3)$$

when [B] is varied by keeping all other parameters constant

$$\frac{V_i}{V_{max}} = \frac{[B]}{K_{m(B)} + [B](1 + K_{m(A)}/[A] + K_{m(A)}[B]/K} \quad (4.4)$$

where [A] is the initial concentration of oleic acid, [B] the initial concentration of butanol, $K_{m(A)}$ the Michaelis Menten constant for oleic acid, $K_{m(B)}$ the Michaelis Menten constant for butanol, K_{1B} the inhibition constant for B, V_i the initial rate of reaction and V_{max} the maximum rate of reaction.

Figure 4.20 shows the Lineweaver – Burk double reciprocal plot for esterification reaction with variation of oleic acid concentrations at different concentration of butanol. The results of the experiments show that the highest initial reaction rates are reached if the substrates are present in equimolar amounts (1:1 molar ratio) in the particular esterification conditions. Hence, by creating a Lineweaver-Burk plots, the values for K_m and V_{max} can be estimated from a regression line through the values for 1/initial rate versus 1/[substrate]. At lower concentration of butanol, the lines are parallel, indicating a Ping Pong Bi Bi mechanism with inhibition by butanol. Furthermore, the lines do not intersect at a common point, which rules out the ternary complex formation. The plots also show that as the concentration of butanol is increased, the slope of the lines with butanol as parameter increases and the intercept on the y-axis (1/ V_i axis) decreases to a limit of 1/ V_{max}. Thus, the results are in consonance with the assumed of Ping Pong Bi Bi mechanism with dead-end-inhibition by butanol. Table 4.3 showed the kinetic constants obtained for the enzymatic esterification of butyl oleate.

Table 4.4: Kinetic constants obtained from Lineweaver-Burl Plot for the enzymatic esterification of butyl oleate

Kinetic constants	Immobilized lipases			
	Native CRL	CMC-CRL	PVA-CRL	PVA:CMC - CRL
[a]V_{max} (butanol) (mmol $^{-1}$.L.min.mg)	$2.056x10^{18}$	1.242×10^{14}	8.088×10^{26}	2.631×10^{12}
[b]V_{max} (oleic acid) (mmol $^{-1}$.L.min.mg)	7.56510^{17}	3.975×10^{19}	1.023×10^{24}	$1.749 x10^{12}$
[a]K_m(butanol) (mmol^{-1}.L)	$4.795x10^{23}$	$2.492x 10^{19}$	$1.754x 10^{32}$	$5.329 x10^{17}$
[b]K_m(oleic acid) (mmol^{-1}.L)	$4.507x10^{23}$	$1.734 x10^{25}$	$4.288 x10^{29}$	$7.28 x10^{17}$

[a]Constant [Oleic acid].Varied [Butanol]; [b]Constant [Butanol].Varied [Oleic Acid]

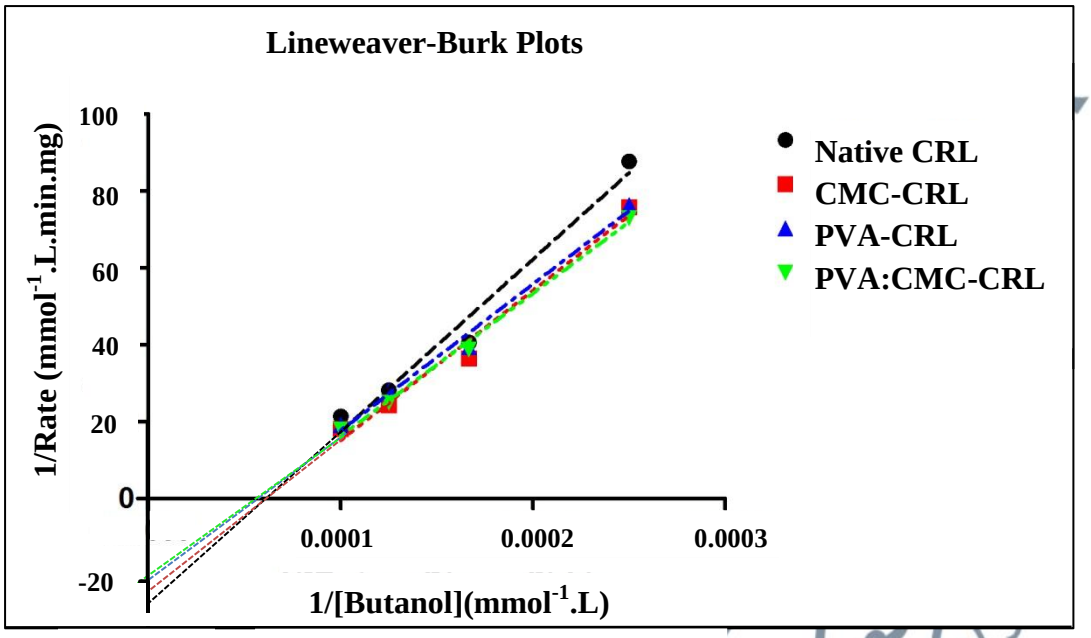

Figure 4.20: Double reciprocal plots of initial rates for butyl oleate synthesis at different Butanol concentrations and constant Oleic acid concentration for Native, CMC-CRL, PVA-CRL and PVA:CMC-CRL.

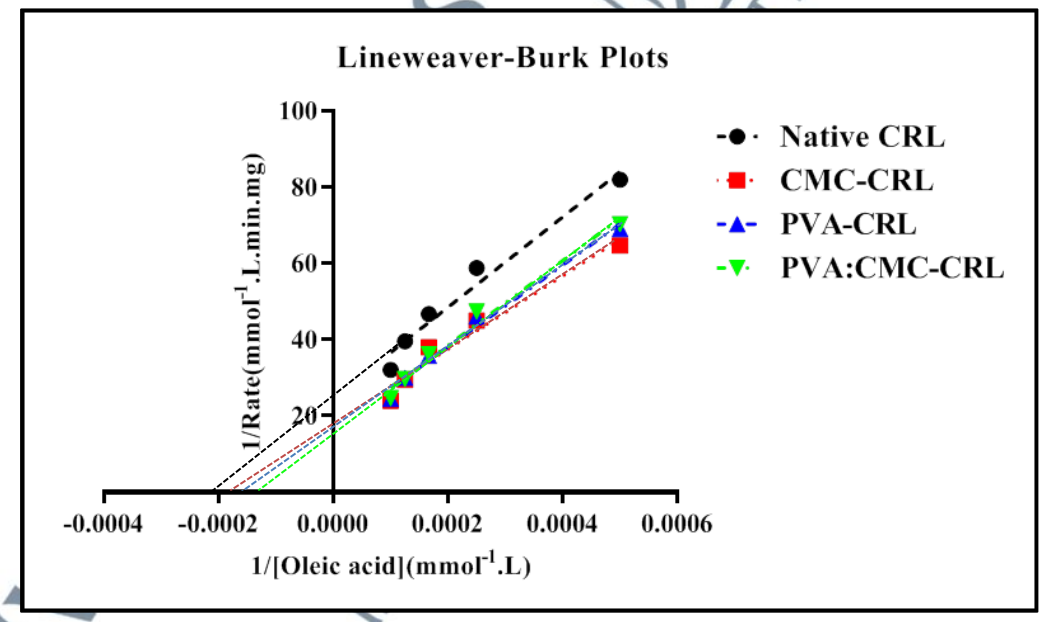

Figure 4.21: Double reciprocal plots of initial rates for butyl oleate synthesis at different Oleic acid concentrations and constant Butanol concentration for Native, CMC-CRL, PVA-CRL and PVA:CMC-CRL.

Ping Pong Bi Bi mechanism involves binding acid with an alcohol in successive steps, which is followed by the release of water and the ester products in succession. The kinetic behaviour of CRL in the esterification of oleic acid and butanol follows the Ping Pong Bi Bi mechanism in which the binding of acid leads an acyl enzyme complex to follow by the release of water molecules. The subsequent binding of alcohol leads to an acyl group to the alcohol, which results in butyl oleate ester formation. In this typical reaction sequence, the lipase may react with butanol to yield a dead-end enzyme-butanol complex or it may react with oleic acid to yield the effective lipase-oleic acid complex. Then the lipase-oleic acid complex transforms to a carboxylic acid-lipase (enzyme-acyl) intermediate and water is released. This is followed by the interaction of carboxylic-lipase with butanol to form another binary complex, which then yields the ester and free lipase (Somashekar et al., 2007).

The Scheme 4.1,4.2 and 4.3 show that the kinetics could be best described by Ping Pong Bi Bi model, in which Butanol and oleic acid bind in subsequent steps that release water butyl oleate ester. This also occurs in subsequent steps with competitive substrate inhibition that leads to dead-end inhibition. This model could be described by the rate equation

$$\frac{V_i}{V_{max}} = \frac{[A][B]}{K_{m(B)}[A](1+[A]/K_{1B})+K_{m(B)}[A]+[A][B]} \quad (4.5)$$

Where V_i is the initial rate, V_{max} is the maximum velocity, [A] is butanol concentration, [B] is oleic acid concentration, $K_{m(B)}$ is Michaelis Menten constant for the lipase, CRL. Butanol complex, K_{1B} is the dissociation constant for the lipase inhibitor (CRL.Oleic acid) complex and $K_{m(B)}$ is Michaelis Menten constant.

Scheme 4.1: Ping Pong Bi Bi Mechanism Pattern with One Substrate (Butanol)

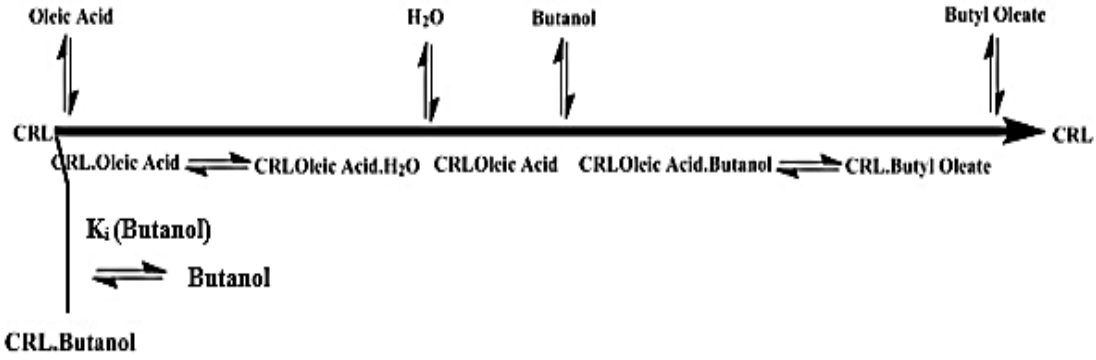

Scheme 4.2: Ping Pong Bi Bi mechanism pattern with one substrate (oleic acid)

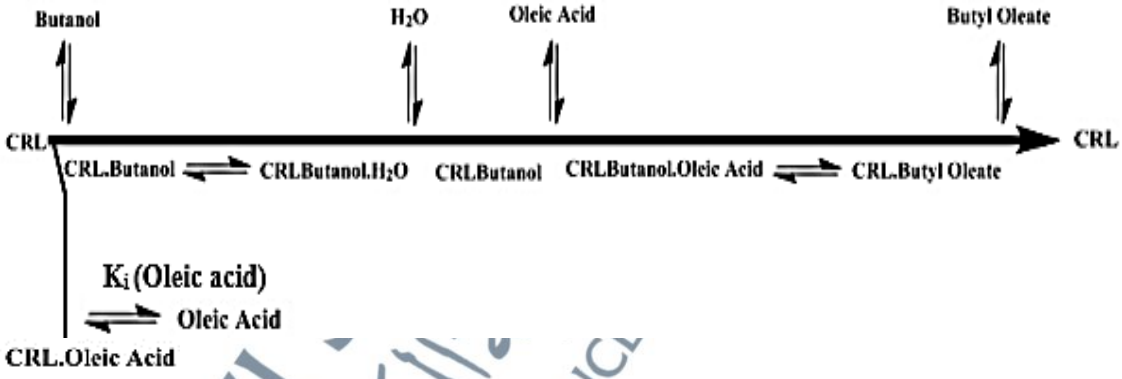

Scheme 4.3: Ping Pong Bi Bi mechanism pattern with two substrates